PHYSICAL REVIEW D **87,** 073003 (2013)

$ZZ\gamma$ and $Z\gamma\gamma$ anomalous couplings in γp collision at the LHC

A. Senol*

Department of Physics, Kastamonu University, 37100 Kastamonu, Turkey and Department of Physics, Abant Izzet Baysal University, 14280 Bolu, Turkey

(Received 30 January 2013; published 8 April 2013)

We study the sensitivity of anomalous $ZZ\gamma$ and $Z\gamma\gamma$ vertex couplings $h_3^{\gamma,Z}$ and $h_4^{\gamma,Z}$, which would be a powerful sign of new physics, via the subprocess $\gamma q \to Zq$ of the main reaction $pp \to p\gamma p \to ZqX$ at the LHC. We calculated limits on these couplings at 95% confidence level for various values of integrated luminosity. It is shown that the $pp \to p\gamma p \to ZqX$ reaction provides 1 order of magnitude improvement in the couplings $h_4^{\gamma,Z}$ compared to the current experimental limits obtained in events dominated by $Z\gamma$ production from the LHC and Tevatron.

DOI: 10.1103/PhysRevD.87.073003 PACS numbers: 12.15.Ji, 12.15.−y, 12.60.Cn

I. INTRODUCTION

The gauge boson self-interactions are determined by the non-Abelian $SU(2)_L \times U(1)_Y$ gauge group of the electroweak sector in the Standard Model (SM). Precision measurements of these interactions will be important for the test of the SM structure. The tree-level couplings between the Z boson and the photon ($ZZ\gamma$ and $Z\gamma\gamma$) vanish in the SM. Any detected signals of these couplings being from the SM expectations within the experimental precision would provide crucial clues for new physics beyond the SM. These new physics effects are parametrized at higher energies via an effective Lagrangian which reduces to the SM at low energies.

The most general anomalous trilinear $Z\gamma Z$ vertex function, being consistent with Lorentz and $U(1)_{\rm em}$ gauge invariance, is given by [1,2]

$$\Gamma^{\alpha\beta\mu}_{Z\gamma Z}(p_1,p_2,p_3) = \frac{p_3^2 - p_1^2}{m_Z^2}\Big[h_1^Z (p_2^\mu g^{\alpha\beta} - p_2^\alpha g^{\mu\beta}) + \frac{h_2^Z}{M_Z^2} p_3^\alpha [(p_3\cdot p_2) g^{\mu\beta} - p_2^\mu p_3^\beta] + h_3^Z \epsilon^{\mu\alpha\beta\rho} p_{2\rho} + \frac{h_4^Z}{m_Z^2} p_3^\alpha \epsilon^{\mu\beta\rho\sigma} p_{3\rho} p_{2\sigma} \Big], \quad (1)$$

where m_Z denotes the Z-boson mass. Formalism of this vertex is depicted in Fig. 1, where e is the charge of the proton. Further, the photon and Z boson in the final state are on shell while the Z boson in the initial state is off shell. The most general $Z\gamma\gamma$ vertex function can be obtained from Eq. (1) with the replacements

$$\frac{p_3^2 - p_1^2}{m_Z^2} \to \frac{p_3^2}{m_Z^2}, \qquad h_i^Z \to h_i^\gamma, \qquad i = 1,\ldots,4. \quad (2)$$

Here the overall factor p_3^2 in the $Z\gamma\gamma$ vertex function results in electromagnetic gauge invariance, while the factor $p_3^2 - p_1^2$ in the $Z\gamma Z$ vertex function [Eq. (1)] ensures Bose symmetry.

The h_i^Z and h_i^γ coupling constants in Eq. (1) have to be described by means of the energy-dependent form factors in a dipolelike form due to the restriction of the $ZZ\gamma$ and $Z\gamma\gamma$ couplings to their SM values at high energies at tree-level unitarity [3–5]. Following Ref. [2], the generalized dipolelike form factors are described:

$$h_i^V(\hat{s}) = \frac{h_{i0}^V}{(1 + \hat{s}/\Lambda^2)^3}; \qquad i = 1,3 \quad (3)$$

$$h_i^V(\hat{s}) = \frac{h_{i0}^V}{(1 + \hat{s}/\Lambda^2)^4}; \qquad i = 2,4. \quad (4)$$

$h_{3,4}^V (h_{1,2}^V)$ couplings are CP conserving (CP violating). All the h_i^V couplings vanish at the tree level in the SM. The CP-violating couplings always cause completely imaginary amplitudes that do not interfere with amplitudes of SM diagrams; thus, we are interested in the CP-conserving couplings. Also, we assume that the new physics scale Λ is above the collision energy $\sqrt{\hat{s}}$ to neglect the energy dependence of the form factors.

The 95% C.L. intervals for anomalous $ZZ\gamma$ and $Z\gamma\gamma$ couplings have been provided by ATLAS [6] for an integrated luminosity ($L_{\rm int}$) of 1.02 fb^{-1} and $\Lambda = \infty$, CMS [7] for $L_{\rm int} = 36$ pb^{-1} and $\Lambda = \infty$, D0 [8] for $L_{\rm int} = 7.2$ fb^{-1} and $\Lambda = \infty$, CDF [9] for $L_{\rm int} = 5.1$ fb^{-1} and $\Lambda = 1.5$ TeV and LEP [10] obtained from $Z\gamma$ events which are given in Table I.

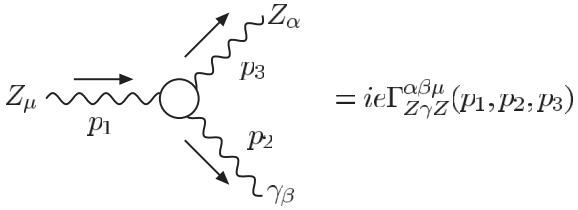

FIG. 1. Feynman rule for the $ZZ\gamma$ vertex.

*asenol@kastamonu.edu.tr

TABLE I. Summary table of limits at the 95% C.L. on anomalous $ZZ\gamma$ and $Z\gamma\gamma$ couplings from $Z\gamma$ events.

Parameters	ATLAS	CMS	D0	CDF	LEP
h_3^γ	$(-0.028, 0.027)$	$(-0.07, 0.07)$	$(-0.027, -0.027)$	$(-0.022, 0.020)$	$(-0.049, 0.008)$
h_3^Z	$(-0.022, 0.026)$	$(-0.05, 0.06)$	$(-0.026, 0.026)$	$(-0.020, 0.021)$	$(-0.20, 0.07)$
h_4^γ	$(-0.00021, 0.00021)$	$(-0.0005, 0.0006)$	$(-0.0014, 0.0014)$	$(-0.0008, 0.0008)$	$(-0.002, 0.034)$
h_4^Z	$(-0.00022, 0.00021)$	$(-0.0005, 0.0005)$	$(-0.0013, 0.0013)$	$(-0.0009, 0.0009)$	$(-0.05, 0.12)$

Probing on $ZZ\gamma$ and $Z\gamma\gamma$ couplings has been studied in the pp [2,11–13], e^+e^- [14–20], and ep [21,22] colliders. In this work, we focus on limits of the anomalous h_3^V and h_4^V couplings via the subprocess $\gamma q \to Zq$ of the main reaction $pp \to p\gamma p \to ZqX$ at the LHC. Here, the quasireal photons emitted from one proton beam are described by equivalent photon approximation (EPA) [23,24] and can interact with quarks coming from the other proton beam. Any process in a γ-proton collision is different from the pure deep inelastic scattering process as a result of two distinctive experimental features. Namely, the first feature is the quasireal photons emitted from the proton have a low virtuality and are scattered with small angles from the beam pipe in the framework of EPA, and for this reason photon-emitting intact protons get away from the central detector without being detected. This leads to a reduction in the energy deposit in the corresponding forward region. Therefore, one of the forward regions of the central detector has a considerable lack of energy, i.e., forward rapidity gaps. Applying a selected cut on this quantity, ordinary pp deep inelastic processes can be sorted out. Another feature is provided by forward detectors. Particles with large pseudorapidity can be detected from forward detectors. If the intact proton emitting a photon is scattered with a large pseudorapidity, it escapes from the central detectors. These protons leave a characteristic sign in the forward detectors for γ-proton collision. These features increase interest in probing new physics via photon-induced processes at the LHC in the literature [25–33].

II. THE CROSS SECTIONS OF THE SUBPROCESS $\gamma q \to Zq$

The subprocess $\gamma q \to Zq$ of the main reaction $pp \to p\gamma p \to ZqX$ at the tree level receives contributions from four Feynman diagrams, as shown in Fig. 2. The last two diagrams account for the anomalous $Z\gamma\gamma$ and $ZZ\gamma$ couplings, and the others depict the SM contributions. The total cross section for the subprocess $\gamma q \to Zq$ is obtained by integrating the cross sections over the photon and quark distributions, where $q = u, \bar{u}, d, \bar{d}, b, \bar{b}, s, \bar{s}, c, \bar{c}$. All calculations were performed by means of the computer package CalcHEP [34], after implementation of the vertex functions Eq. (1). During calculations, we use parton distribution functions library CTEQ6L [35] and the photon spectrum in the EPA [23] embedded in CalcHEP.

The photon spectrum in EPA as a function of photon energy E_γ and its virtuality Q^2 is given by the following formula [23,32,36]:

$$\frac{dN_\gamma}{dE_\gamma dQ^2} = \frac{\alpha}{\pi}\frac{1}{E_\gamma Q^2}\left[\left(1-\frac{E_\gamma}{E}\right)\left(1-\frac{Q^2_{\min}}{Q^2}\right)F_E + \frac{E_\gamma^2}{2E^2}F_M\right], \tag{5}$$

where α is the fine structure constant, and $Q^2_{\min}$, standing for the minimum photon virtuality, is given by

$$Q^2_{\min} = \frac{m_p^2 E_\gamma^2}{E(E-E_\gamma)}.$$

Here, m_p is the mass of the proton and E denotes the energy of the incoming proton beam. The functions of the electric and magnetic form factors F_E and F_M are displayed by

$$F_E = \frac{4m_p^2 G_E^2 + Q^2 G_M^2}{4m_p^2 + Q^2}, \qquad F_M = G_M^2$$

$$G_E^2 = \frac{G_M^2}{7.78} = \left(1 + \frac{Q^2}{0.71\ \text{GeV}^2}\right)^{-4}.$$

The cross section of the process $pp \to p\gamma p \to ZqX$ can be expressed by integrating the cross section for the subprocess $\gamma q \to Zq$ over the photon and quark spectra

$$\sigma(pp \to p\gamma p \to ZqX) = \int_{Q^2_{\min}}^{Q^2_{\max}} dQ^2 \int_{x_{1\min}}^{x_{1\max}} dx_1 \int_{x_{2\min}}^{x_{2\max}} dx_2 \left(\frac{dN_\gamma}{dx_1 dQ^2}\right) \times \left(\frac{dN_q}{dx_2}\right)\hat{\sigma}_{\gamma q \to Zq}(\hat{s}), \tag{6}$$

where $x_1 = \frac{E_\gamma}{E}$, and x_2 is the momentum fraction of the proton's momentum carried by the quark when $\frac{dN_q}{dx_2}$ is the

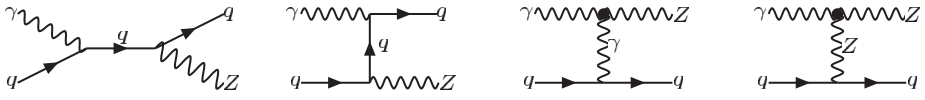

FIG. 2. Tree-level Feynman diagrams for the subprocess $\gamma q \to Zq$ ($q = u, \bar{u}, d, \bar{d}, b, \bar{b}, s, \bar{s}, c, \bar{c}$).

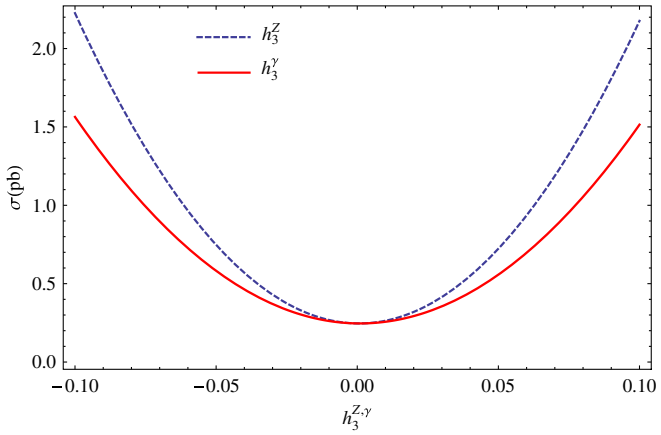

FIG. 3 (color online). The total cross sections depending on anomalous h_3^γ and h_3^Z couplings for the subprocess $\gamma q \to Zq$ with taking $\sqrt{s} = 14$ TeV.

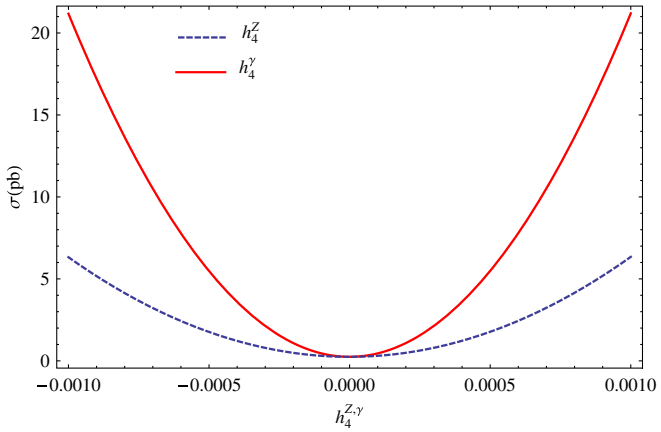

FIG. 4 (color online). The total cross sections depending on anomalous h_4^γ and h_4^Z couplings for the subprocess $\gamma q \to Zq$ with taking $\sqrt{s} = 14$ TeV.

quark distribution function of the proton. We have considered photon virtuality $\langle Q^2 \rangle \approx 0.01$ GeV^2, due to the low virtuality of the emitted photons in the EPA [36]. In our calculations, we set $Q^2_{\max} = 2$ GeV^2 for which the contribution to the integral above this value is negligible.

In Figs. 3 and 4, we plot the total cross section of the subprocess $\gamma q \to Zq$ as a function of anomalous $h_3^{\gamma,Z}$ and $h_4^{\gamma,Z}$ couplings at the center of mass energy of 14 TeV. In these figures, only one of the anomalous couplings is kept to be different from zero. As seen from the figures, cross sections for h_3^Z couplings are larger as compared to h_3^γ. In contrast, the cross sections for h_4^γ couplings are larger than those of h_4^Z couplings. This is related to the fact that the dependencies of the terms of h_3^Z (h_4^Z) and $h_3^\gamma(h_4^\gamma)$ on the matrix element squared are not the same, because of the presence of the different overall factors in the vertex functions.

III. LIMITS ON THE ANOMALOUS $ZZ\gamma$ AND $Z\gamma\gamma$ COUPLINGS

One-dimensional and two-dimensional χ^2 tests were applied without a systematic error to obtain 95% C.L. on the upper limits of anomalous $h_3^{\gamma,Z}$ and $h_4^{\gamma,Z}$ couplings. The χ^2 function is

$$\chi^2 = \left(\frac{\sigma_{SM} - \sigma_{AN}}{\sigma_{SM}\delta}\right)^2, \tag{7}$$

where $\delta = \frac{1}{\sqrt{N}}$ is the statistical error. The number of events are given by $N = S \times E \times \sigma_{SM} \times L_{\text{int}} \times \text{BR}(Z \to l\bar{l})$, where S is the survival probability factor, E denotes the jet reconstruction efficiency, L_{int} is the integrated luminosity, and $l = e^-$ or μ^-. When calculating the number of events we assume $S = 0.7$ and $E = 0.6$ for our process, the same as in Ref. [32]. Because of the overwhelming four jet QCD background, Z bosons decaying hadronically are not considered here. We applied both cuts for the transverse momentum of final state quarks to be $p_T^j > 15$ GeV and the pseudorapidity of final state quarks to be $|\eta| < 2.5$, because ATLAS and CMS have central detectors with a pseudorapidity coverage $|\eta| < 2.5$.

If a lower cut is applied on the transverse momentum of scattered protons emitting photons in a photoproduction process, such a cut helps us to discern a photoproduction process deduced from the usual pp backgrounds, since the transverse momenta of the scattered protons are typically $p_T \lesssim 1$ GeV [28]. Therefore, the transverse momentum of an outgoing proton to be $p_T > 0.1$ GeV within the photon spectrum is applied.

According to these restrictions, we have calculated $\sigma_{SM} = 0.39$ pb for $\gamma q \to Zq$ ($q = u, \bar{u}, d, \bar{d}, b, \bar{b}, s, \bar{s}, c, \bar{c}$) at $\sqrt{s} = 14$ TeV. In Table II, we present 95% C.L. sensitivity limits on $h_3^{\gamma,Z}$ and $h_4^{\gamma,Z}$ for various integrated luminosities by varying one coupling at a time.

TABLE II. One-dimensional limits on $ZZ\gamma$ and $Z\gamma\gamma$ coupling parameters at 95% C.L. for the subprocess $\gamma q \to Zq$ with taking $\sqrt{s} = 14$ TeV.

L(fb^{-1})	h_3^Z	h_4^Z	h_3^γ	h_4^γ
30	(− 0.016, 0.018)	(− 0.000099, 0.000098)	(− 0.019, 0.022)	(− 0.000053, 0.000053)
50	(− 0.014, 0.016)	(− 0.000088, 0.000086)	(− 0.017, 0.020)	(− 0.000047, 0.000046)
100	(− 0.012, 0.013)	(− 0.000074, 0.000072)	(− 0.014, 0.017)	(− 0.000039, 0.000039)
200	(− 0.009, 0.011)	(− 0.000062, 0.000061)	(− 0.012, 0.014)	(− 0.000033, 0.000033)

The background considered above comes from the subprocess $\gamma q \to Zq$, of which the final state is composed of an admixture of light quarks and jets, and dileptons originating from $Z \to l^+ l^-$. In the case of b tagging we assume the efficiency of 60%, and the miss-tagging factors for c quarks and light quarks are taken as 10% and 1%, respectively.

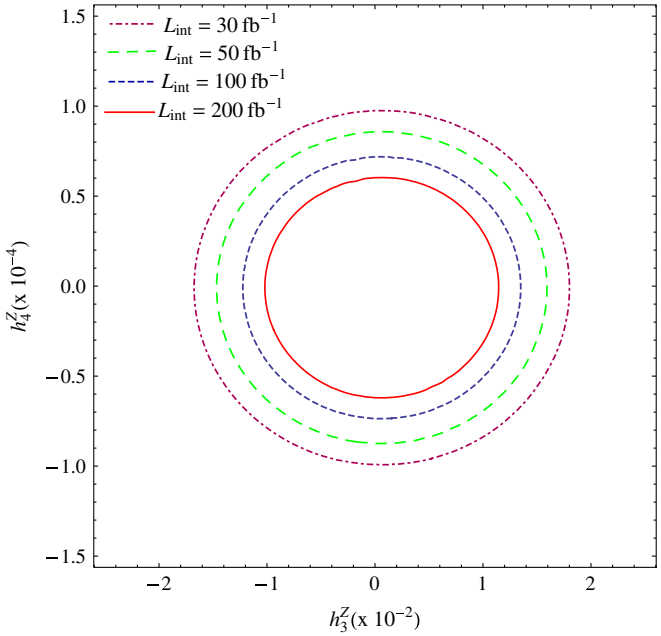

FIG. 5 (color online). Two-dimensional 95% limit contour for anomalous h_3^Z and h_4^Z couplings for the subprocess $\gamma q \to Zq$ with taking $\sqrt{s} = 14$ TeV.

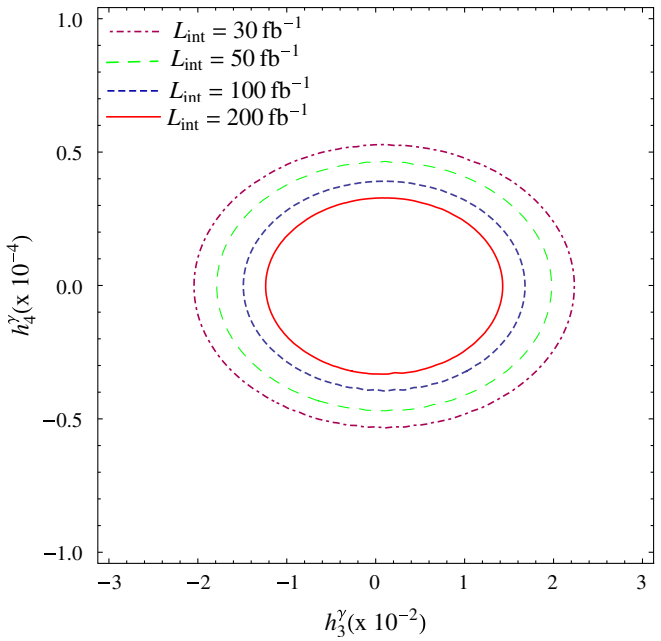

FIG. 6 (color online). Two-dimensional 95% limit contour for anomalous h_3^γ and h_4^γ couplings for the subprocess $\gamma q \to Zq$ with taking $\sqrt{s} = 14$ TeV.

Taking all these criteria, the background cross section is diminished by 2.1%. Then, the sensitivity of our bounds are spoiled by about a factor of 1.75. To illustrate, the bounds on h_4^γ and h_4^Z became $(-0.000069, 0.000069)$ and $(-0.00013, 0.00013)$ for $L_{\rm int} = 100\ {\rm fb}^{-1}$, respectively. Besides, the other source of backgrounds is the instrumental background arising from the calorimeter noise. The calorimeter noise can be prohibited with a suitable cut on the transverse energy of jets (e.g., $E_T > 40$ GeV).

When comparing these limits with the experimental bounds given in Table I, we can see that the bounds on $h_3^{\gamma,Z}$ in the unitarity violation scheme obtained from ATLAS, D0, and CDF are of the same order as our bounds, while the $h_4^{\gamma,Z}$ limits are 1 order weaker than our limits. In addition, we show two-dimensional 95% C.L. limit contours for $ZZ\gamma$ vertex couplings h_3^Z and h_4^Z in Fig. 5 and for $Z\gamma\gamma$ vertex couplings h_3^γ and h_4^γ in Fig. 6 at $\sqrt{s} = 14$ TeV for various integrated luminosities. Because of the fact that the $h_4^{Z,\gamma}$ couplings come from dimension-eight operators, the bounds are more restricted than those of $h_3^{Z,\gamma}$ which stem from dimension-six.

IV. CONCLUSIONS

We have examined the model-independent parametrization of anomalous $ZZ\gamma$ and $Z\gamma\gamma$ vertex couplings h_3^V and h_4^V within the effective operator approach via the subprocess $\gamma q \to Zq$ of the main reaction $pp \to p\gamma p \to ZqX$ at the LHC with a center of mass energy of 14 TeV. The potential of the LHC to probe anomalous $ZZ\gamma$ and $Z\gamma\gamma$ couplings is analyzed via hadronic $Z\gamma$ production at $\sqrt{s} = 14$ TeV with the integrated luminosity of 10 and 100 fb^{-1} [11]. The limits obtained via the $pp \to Z\gamma + X \to \not{p}_T\gamma + X$ process in Ref. [11] are $|h_3^Z| < 1.9 \times 10^{-3}$ (3.4×10^{-3}) and $|h_4^Z| < 1.2 \times 10^{-5}$ (2.5×10^{-5}) at the LHC with $L_{\rm int} = 100(10)$ fb^{-1}. Our results on h_4^V are of the same order with those of Ref. [11] at $L_{\rm int} = 100$ fb^{-1}, while the limits on h_3^V remain 1 order lower. However, a photoproduction process at hadron colliders provides a rather clean channel compared to the pure deep inelastic process due to the detection of scattered protons emitting photons by the forward detectors. Furthermore, the obtained results being related to the anomalous $ZZ\gamma$ and $Z\gamma\gamma$ vertex couplings from a photoproduction process are complementary to traditional pp studies. Nevertheless, if we compare the current experimental limits with the results determined from this work, our limits on the couplings h_4^V with $L_{\rm int} = 30$ fb^{-1} are 1 order better than the experimental limits obtained from LHC and Tevatron as given in Table I, while the h_3^V couplings are of the same order as the current experimental limits.

ACKNOWLEDGMENTS

I would like to thank G. Yildirim and A. T. Tasci for useful discussions and Orhan Cakir for useful comments.

[1] K. Hagiwara, R. D. Peccei, D. Zeppenfeld, and K. Hikasa, Nucl. Phys. **B282**, 253 (1987).
[2] U. Baur and E. L. Berger, Phys. Rev. D **47**, 4889 (1993).
[3] J. M. Cornwall, D. N. Levin, and G. Tiktopoulos, Phys. Rev. Lett. **30**, 1268 (1973); **31**, 572(E) (1973).
[4] J. M. Cornwall, D. N. Levin, and G. Tiktopoulos, Phys. Rev. D **10**, 1145 (1974); **11**, 972(E) (1975).
[5] C. H. Llewellyn and Smith, Phys. Lett. **46B**, 233 (1973).
[6] G. Aad *et al.* (ATLAS Collaboration), Phys. Lett. B **717**, 49 (2012).
[7] S. Chatrchyan *et al.* (CMS Collaboration), Phys. Lett. B **701**, 535 (2011).
[8] V. M. Abazov *et al.* (D0 Collaboration), Phys. Rev. D **85**, 052001 (2012).
[9] T. Aaltonen *et al.* (CDF Collaboration), Phys. Rev. Lett. **107**, 051802 (2011).
[10] J. Alcaraz *et al.* (ALEPH, DELPHI, L3, OPAL, and LEP Electroweak Working Group Collaborations), arXiv:hep-ex/0612034.
[11] U. Baur, T. Han, and J. Ohnemus, Phys. Rev. D **57**, 2823 (1998).
[12] U. Baur and D. L. Rainwater, Phys. Rev. D **62**, 113011 (2000).
[13] D. Choudhury, S. Dutta, S. Rakshit, and S. Rindani, Int. J. Mod. Phys. A **16**, 4891 (2001).
[14] T. G. Rizzo, Phys. Rev. D **54**, 3057 (1996).
[15] R. Walsh and A. J. Ramalho, Phys. Rev. D **57**, 5908 (1998).
[16] R. Walsh and A. J. Ramalho, Phys. Rev. D **65**, 055011 (2002).
[17] S. Atag and I. Sahin, Phys. Rev. D **68**, 093014 (2003).
[18] S. Atag and I. Sahin, Phys. Rev. D **70**, 053014 (2004).
[19] A. Gutierrez-Rodriguez, M. A. Hernandez-Ruiz, and M. A. Perez, Phys. Rev. D **80**, 017301 (2009).
[20] B. Ananthanarayan, S. K. Garg, M. Patra, and S. D. Rindani, Phys. Rev. D **85**, 034006 (2012).
[21] Y. A. Coutinho, A. J. Ramalho, R. Walsh, and S. Wulck, Phys. Rev. D **64**, 115008 (2001).
[22] I. Turk Cakir, Acta Phys. Pol. B **40**, 309 (2009).
[23] V. M. Budnev, I. F. Ginzburg, G. V. Meledin, and V. G. Serbo, Phys. Rep. **15**, 181 (1975).
[24] I. F. Ginzburg, G. L. Kotkin, V. G. Serbo, and V. I. Telnov, Nucl. Instrum. Methods Phys. Res. **205**, 47 (1983).
[25] V. A. Khoze, A. D. Martin, and M. G. Ryskin, Eur. Phys. J. C **23**, 311 (2002).
[26] O. Kepka and C. Royon, Phys. Rev. D **78**, 073005 (2008).
[27] J. de Favereau de Jeneret, V. Lemaitre, Y. Liu, S. Ovyn, T. Pierzchala, K. Piotrzkowski, X. Rouby, and N. Schul *et al.*, arXiv:0908.2020.
[28] M. G. Albrow, T. D. Coughlin, and J. R. Forshaw, Prog. Part. Nucl. Phys. **65**, 149 (2010).
[29] I. Sahin and A. A. Billur, Phys. Rev. D **83**, 035011 (2011).
[30] R. S. Gupta, Phys. Rev. D **85**, 014006 (2012).
[31] I. Sahin, Phys. Rev. D **85**, 033002 (2012).
[32] I. Sahin and B. Sahin, Phys. Rev. D **86**, 115001 (2012).
[33] B. Sahin and A. A. Billur, Phys. Rev. D **86**, 074026 (2012).
[34] A. Belyaev, N. D. Christensen, and A. Pukhov, arXiv:1207.6082.
[35] J. Pumplin, D. R. Stump, J. Huston, H. L. Lai, P. M. Nadolsky, and W. K. Tung, J. High Energy Phys. 07 (2002) 012.
[36] K. Piotrzkowski, Phys. Rev. D **63**, 071502 (2001).